REVISTA MATÉRIA V.29 N.2
ISSN 1517-7076 articles e20240228, 2024

The amorphous phase of $Co_{67}Si_{23}B_{10}$ alloy produced by mechanical alloying

Luciano Nascimento[1], Elvia Leal[1], Danyelle Garcia Guedes[1], Meirilany Rozeno Costa[1], Adriano Lima da Silva[1], Gabryella Garcia Guedes[2], Ana Cristina Figueiredo de Melo Costa[1]

[1]Universidade Federal de Campina Grande, Unidade Acadêmica de Engenharia de Materiais, Laboratório de Síntese dos Materiais Cerâmicos. Av. Aprígio Veloso, 882, 58429-900, Bodocongó, Campina Grande, PB, Brasil.

[2]Universidade Estadual da Paraíba, Laboratório de Desenvolvimento e Caracterização de Produtos Farmacêuticos. Rua das Baraúnas, 351, 58429-500, Bodocongó, Campina Grande, PB, Brasil.

e-mail: luciano.uepb@gmail.com, elvialeal@gmail.com, anyelle.garcia@certbio.ufcg.edu.br, meirycosta.2009@hotmail.com, gaby.garcia@gmail.com, adrianolimadasilva@live.com, ana.costa@ufcg.edu.br

ABSTRACT

In this work, the evolution and formation of the amorphous phase during the preparation of amorphous $Co_{67}Si_{23}B_{10}$ (*at.%*) powder by mechanical alloying (MA) under an argon atmosphere were studied. The grinding time of 15 h had a profound effect on the phase transformation, microstructure, morphology development, and thermal and magnetic behavior of the powders. These effects were studied by X-ray diffraction (XRD), EDX scanning electron microscopy (SEM), thermal analysis (TGA/DTA), N_2 texture analysis (BET/BJH) and, magnetic measurements (VSM). The results show that the evolution of the amorphous phase in the early stage of milling consists of nanocrystalline α-Co_2B and β-Co_2Si phases, which are diluted and coexist with the amorphous phase. After 15 hours of ball milling, the amorphous phase became the main phase with a proportion of 98.1%, which is relatively high compared to the 1.9% of the nanocrystalline phases α-Co_2B and β-Co_2Si. The results obtained indicate that amorphization develops with higher thermal stability than a small fraction of the nanocrystalline phase diluted in the amorphous phase. This behavior suggests the presence of the amorphous phase coexisting with the nanocrystalline phase in a small fraction with overlapping crystallization and recrystallization at a temperature of around 924.42°C.

Keywords: amorphous phase; $Co_{67}Si_{23}B_{10}$ powder; mechanical alloying (MA).

1. INTRODUCTION

Amorphous alloys are a unique class of materials characterized by a lack of long-range structural order ordering while retaining short-range chemical ordering, and they giving them a series of superior physical properties compared to their polycrystalline counterparts [1, 2] . Amorphous alloys also have practical applications due to their unique magnetic properties [3], good mechanical behavior [4], and high corrosion resistance [5], making them suitable for a variety of industrial applications in fields such as energy [6], aeronautics, chemistry [7], and orthopedic biomaterials [8].

The Co-based amorphous alloys exhibit near-zero magnetostriction and magnetocrystalline anisotropy [9], giving them outstanding soft magnetic properties such as low coercivity [10], high permeability [11], low hysteresis losses [12], lower saturation induction and high mechanical strength compared to their crystalline counterparts [13]. This is due to the relatively large amount of metalloid atoms present in their composition. Metalloid elements (B, Si, P, C, and Ge) in order to understand their effects on the atomic structure, glass formation ability (GFA), thermal stability, and magnetic properties of Co-based amorphous alloys [14, 15]. Over the years, several synthesis routes have been used to produce amorphous soft magnetic materials, including melt spinning [16], gas atomization [17], mechanical alloying [18], copper mould casting [19], vapour deposition [20], and plasma processing [21].

Mechanical alloying (MA) is an alternative process for producing amorphous alloys from either a mixture of pure elemental powders [22]. MA offers several advantages over traditional casting or rapid solidification methods. Mechanically alloyed amorphous powders can be easily solidified into high-density amorphous bulk

Corresponding Author: Luciano Nascimento Received on 06/05/2024 Accepted on 13/05/2024

DOI: https://doi.org/10.1590/1517-7076-RMAT-2024-0228

samples of any shape and size in a supercooled liquid region without the need for any post-processing processes such as mechanical processing [23, 24]. Furthermore, MA is versatile enough to allow amorphization over a composition range that is wider than that corresponding to rapid solidification and is close to the eutectic composition [25, 26].

A major advantage of the mechanical alloying route is that this technique can successfully produce amorphous materials in systems where conventional routes, such as melt spinning, fail or are difficult to achieve metallic alloy amorphization evolution [27]. Different authors have demonstrated the effectiveness of mechanical alloying in promoting the amorphization of various Co-based alloys, such as Co–B [28], Co–Si [29], Co-Fe-Si-B-Nb [30], Co-Fe-B-Si-Nb [31], Co–Ta–B [32], and Co–Cr–Mo–Nb–B [33]. On the other hand, the main disadvantage of the MA process is that the balls or milling media introduce impurities and grinding residues into the powder, which may affect the thermal stability and some physical properties of the amorphous powder [34].

The amorphous phase formed by MA depends on the energy provided by the grinding media, the atomic size of the components, and the thermodynamic properties of the alloy system [35]. Currently, two criteria are required for the formation of amorphous phases during MA processes in binary and ternary systems: *(i)* large negative mixing heats between the basic components and *(ii)* large asymmetries in elemental diffusion coefficients [36]. The amorphous phase is kinetically formed when the amorphization reaction occurs much faster than the formation of the nanocrystalline and crystalline phases [37]. It has also been shown that the introduction of crystal defects into the lattice during the MA process increases the internal energy [38]. When the free energy of the crystal exceeds the free energy of the amorphous phase, the crystal structure becomes thermodynamically unstable and can transform into the amorphous phase [39].

In this paper, we report on the preparation of $Co_{67}Si_{23}B_{10}$ (at. %) amorphous powder via a wet mechanical alloying (MA) route. The milling time of 15 h was required for alloy amorphization. The evolution of the morphological and microstructural characteristics of the powder, magnetic properties, and thermal stability of the powders are presented and discussed.

2. MATERIALS AND METHODS

Elemental metallic powders (99.9% purity, from Êxodo Científica−LTDA/Brasil) of Co, Si, and B with a nominal composition of $Co_{67}Si_{23}B_{10}$ (*at. %*) were mechanically alloyed using a planetary ball mill (Type Fritsch Pulverisette 5) under an Ar atmosphere (99.9% purity). To produce this alloy, 20 g of each batch metal powder was stoichiometrically weighed and placed in a grinding bowl made of hardened stainless-steel balls and vials, with seven balls (12 mm diameter), and subjected to a total milling time of 15 h. The mill speed was set at 350 rpm, and the ball-to-powder ratio (BPR) was kept at 20:1. Ethyl alcohol (C_2H_6O) from Sigma-Aldrich Brasil Ltda was used as a process control agent (PCA) to regulate the morphology of the homogenized powder. The microstructural evaluation of the samples obtained from the mechanical alloying was carried out by X-ray diffraction (XRD; BRUKER diffractometer, model D2 Phaser) using CuK_α (λ = 1.54056 Å) radiation produced at 45 kV and 40 mA. The diffraction angle (2θ) was ranging between 10° and 80° with a step size of 0.013°, and a time of 5 s.

Microstructural morphology and chemical composition of the powders milled was evaluated by scanning electron microscope (SEM; TESCAN VEGA3) equipped with the energy dispersive X-ray (EDX), operating at 30 kV with a magnification of 100 kx. In the EDX diagram, the Au element was detected, which was caused by the gold spraying treatment to the sample before the test. Thermal studies of the milled amorphous powder $Co_{67}Si_{23}B_{10}$ were collected after milling using differential thermal analysis (DTA) and thermogravimetric analysis (TGA) equipment from the brand SHIMADZU DTG-60H. All thermal studies were conducted under argon atmosphere with a heating rate of 10°C/min. Textural analysis was conducted using a Quantachrome NOVA 2200E BET surface area and pore size analyzer, model Autosorb IQ, to obtain adsorption/desorption isotherms of the amorphous alloy $Co_{67}Si_{23}B_{10}$. The uniaxial compressive mechanical tests were conducted on a WDW-100 testing machine at a strain rate of $4\ 10^{-4}\ s^{-1}$ at room temperature. The size of the $Co_{67}Si_{23}B_{10}$ powder pressed into a cylindrical disc shape is 2 mm in diameter and 4mm in height. The compression tests were performed at least in triplicate for the $Co_{67}Si_{23}B_{10}$ powder. Magnetic properties were studied by a vibrating sample magnetometer (VSM) at 25°C within a ± 40 kOe magnetic field range.

3. RESULTS AND DISCUSSION

Figure 1 displays the X-ray pattern of $Co_{67}Si_{23}B_{10}$ powder during milling time of 15 h. The diffraction pattern contains of a diffuse halo that includes the amorphous phase and small two diffraction reflections corresponding to the nanocrystalline phases of the α-Co_2B and β-Co_2Si type [40] in Figure 1.

A broad diffusion peak near 2θ = 45º suggests the presence of an amorphous structure in the prepared $Co_{67}Si_{23}B_{10}$ powder, as illustrated in Figure 1 obtained by MA. The nanocrystalline α-Co_2B and β-Co_2Si phases showed a weak reflection that corresponds to 1.9%. It indicates that they are embedded in the amorphous matrix with a larger fraction of 98.1% in this phase. Thus, nanocrystals were formed under strain with an average size of 30 nm during the MA process of powder milling [41].

Figure 2 shows the SEM/EDS micrograph of the amorphous powder $Co_{67}Si_{23}B_{10}$. A particle morphology is observed with shapes of irregular aggregates of snowflakes and small flat spheres with a typical size of 50 μm [42].

In the upper right corner of Figure 2, a small spherical particle flattened at the poles with a typical size of 20 μm is visible, indicating strong plastic deformation effects during the 15 h milling process, leading to the evolution of the amorphous phase in the structural composition. By milling for 15 h as illustrated in Figure 2, we observe that, the powders are strain-hardened by heavy plastic deformation during milling and become brittle in nature [43]. In this case, no agglomeration and cold welding occur due to fracturing mechanisms. As a result, the particle size is reduced, producing a mixture of semi-spherical and flattened particles, as can be seen at the top of the SEM micrograph in Figure 2. A narrow size distribution of 20 μm is developed.

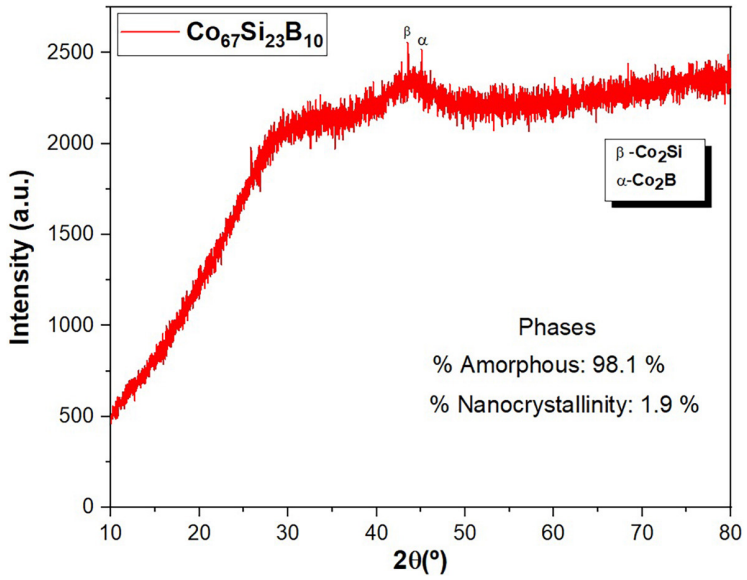

Figure 1: XRD pattern of $Co_{67}Si_{23}B_{10}$ powder.

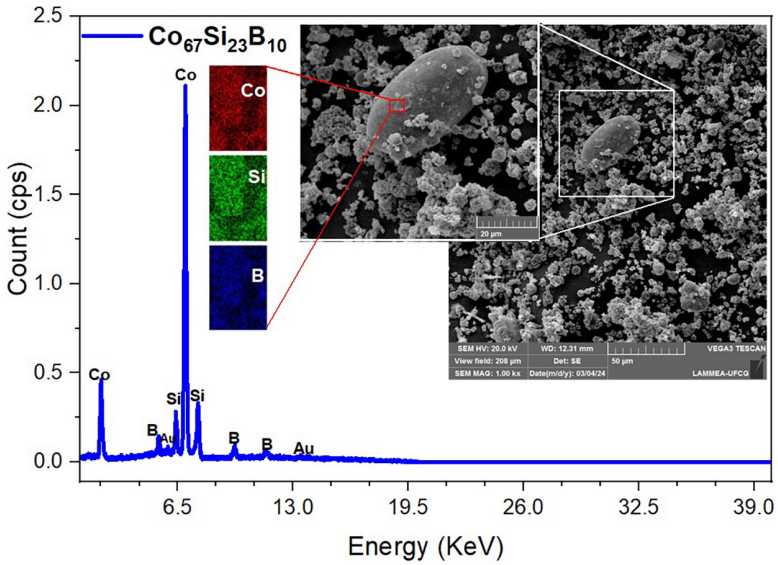

Figure 2: SEM/EDS micrographs of the $Co_{67}Si_{23}B_{10}$ powder.

Figure 2 displays the EDS analysis and mapping of the powder that was obtained after 15 h of milling. Co, Si, and B were present in the initial mixture, according to the EDS analysis. However, the EDS mapping reveals that the powders became inhomogeneous, and distinct clusters of Co, Si and B indicate the development of small fractions of nanocrystalline phases α-Co_2B and β-Co_2Si diluted and coexisting with the amorphous phase towards the end result of the amorphous powder $Co_{67}Si_{23}B_{10}$ mixture during milling [44].

Figure 3 shows the TGA-DTG curves of $Co_{67}Si_{23}B_{10}$ powder obtained by heating until 1000ºC under an Ar atmosphere.

According to Figure 3, it can be said that the amorphous $Co_{67}Si_{23}B_{10}$ powder remains an amorphous metallic alloy up to a temperature of approximately 449.44°C, where a mass loss of only 1.03% occurs, which can be attributed to the loss of adhered moisture in conjunction with the presence of some reducible oxides, burnt carbon, etc.

Subsequently, in the temperature range of 449.44°C–672.56°C, a small mass gain of 5.676% is observed, showing the beginning of the crystallization and phase transformation of the amorphous $Co_{67}Si_{23}B_{10}$ powder. It also indicated that the crystallization was followed by the high temperature oxidation with some mass gains. The onset temperatures of the first and second exothermic peaks (T_{x1} and T_{x2}) obtained from Figure 3.

For each curve, two separate exothermic peaks can be recognized, indicating a two-stage crystallization behavior. To clarify the precipitation phases, the structures of the alloys milled for 15 h under the effect of grinding in a wet environment were examined by XRD. Two of these peaks are the primary and secondary crystallization temperatures, where the formation of crystals from the amorphous phase is observed during the oxidation process.

The other two peaks show the oxidation transformation in the ribbons, and one of them shows a phase transformation. In region I, the exothermic peak in the DTA curve occurs around 675.87°C. After 15 h of milling time, a phase transition occurs. Heating the $Co_{67}Si_{23}B_{10}$ powder to higher temperatures leads to the formation of stable α-Co_2B and β-Co_2Si from the residual disordered phase [45, 46]. The phase of the $(Co, Si)_3B$ type is retained in this case. The glass transition temperature (T_{g1}) is about 637.59°C and the first crystallization temperature (T_{x1}) is around is around 675.87°C for the amorphous $Co_{67}Si_{23}B_{10}$ powder, which corresponds to the supercooled liquid region associated to the endothermic peak, being considered higher value of ΔT causes a growth delay in the grain, i.e. $\Delta T_1 = T_{x1} - T_{g1}$ =38.28°C with bulk metal glasses (BMG) of the cycle I region dotted in red. In the last stage of region II, we observed an exothermic peak in the DTA at ~924.42°C, α-Co_2B and β-Co_2Si can be fixed in the phase composition of the alloy to a stable crystalline state through the mechanism

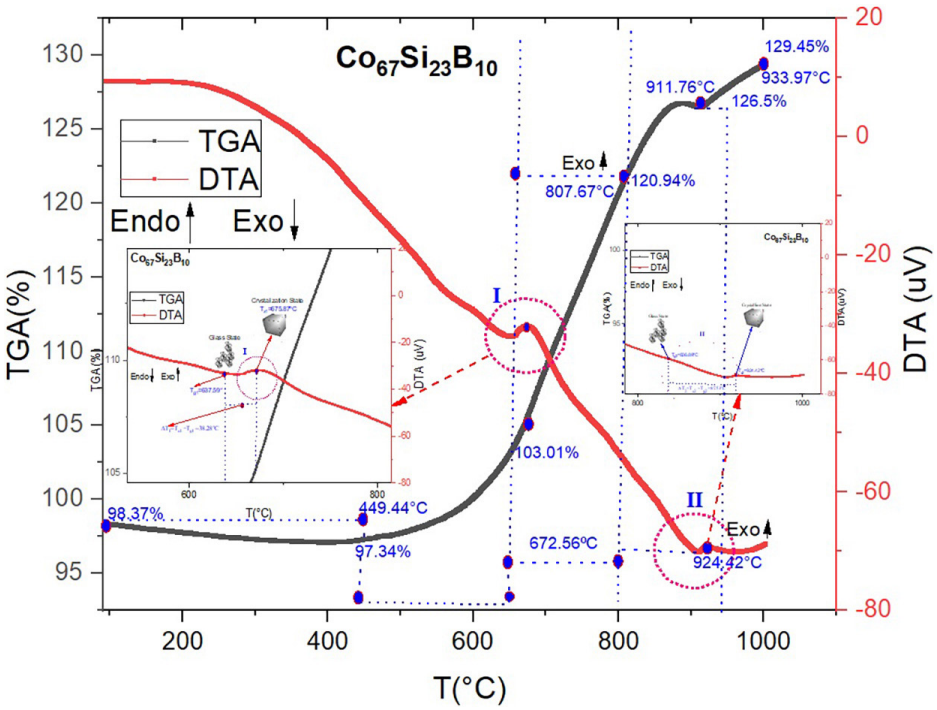

Figure 3: Overlapping TGA/DTA curves of the $Co_{67}Si_{23}B_{10}$ powder.

of crystal nucleation and growth [47, 48]. Thus, the comparative study of the peculiarities of the crystallization and thermal stability of amorphous phases produced by MA. In circle II, the glass transition temperature (T_{g2}) is about 836.89°C, and the first crystallization temperature (T_{2x}) is around 924.42°C for the amorphous $Co_{67}Si_{23}B_{10}$ powder [49]. The supercooled liquid region of circle II is associated with the endothermic peak by a temperature higher value of ΔT_2 causes a growth delay in the grain, i.e., $\Delta T_2 = T_{x2} - T_{g2}$ = 87.53°C with bulk metal glasses (BMG) [50, 51].

The transition to a stable crystalline state upon heating occurs through the mechanism of crystal nucleation and growth [52, 53]. Under the effect of a thermodynamic driving force, such a process can be realized, depending on the kinetic features, either through the formation of stable crystals directly from the amorphous phase or, if this way is kinetically hindered, through the formation of a number of metastable crystal structures [54, 55]. It is known that plastic deformation of an amorphous phase increases the fraction of excess free volume in it, which facilitates the diffusion of atoms [56]. Consequently, in the MA amorphous alloys, we can expect, because of an increased excess free volume, the acceleration of diffusion, the elimination of kinetic restrictions, a decrease in thermal stability, and a simpler mechanism of crystallization (amorphous phase→stable crystalline phase) compared to the amorphous ribbons of the same chemical composition of the amorphous alloy [57, 58].

Figure 4 shows the $Co_{67}Si_{23}B_{10}$ powder with isothermal type IV adsorption lines and H3-type hysteresis loops. The hysteresis loops of the black and red lines represent the adsorption (ADS) and desorption (DES) curves.

Furthermore, they presented type IV isotherm profiles as shown in Figure 4, indicating mesoporous properties due to their high mesopore density according to the IUPAC classification [59]. The pore structure is provided by the aggregates of small powders in flake-like shapes and small spherical particles flattened with a maximum specific surface area of 3.195 m^2/g and an average pore size of the adsorbent reached 1.0505 nm, respectively.

Figure 5 shows the hysteresis loops M-H for the powder $Co_{67}Si_{23}B_{10}$ at temperatures of 300 K, respectively, with a magnetic field range of –15 kOe to 15 kOe.

The hysteresis loop M-H of the powder $Co_{67}Si_{23}B_{10}$ shows an estimated saturation magnetization M_s = 114.31 emu/g, remanent magnetization M_r = 7.27 emu/g, and a coercive field H_c = 0.04869 kOe. In the upper part of Fig. 5, it exhibits strong typical soft magnetic alloy characteristics after milling the powder for 15 h. It is observed that the saturation remanence ratio (M_r/M_s) of powder $Co_{67}Si_{23}B_{10}$ is 0.05144, i.e., multidomains ($M_r/M_s << 0.1$) during 15 h of milling. The milled powders display the same ferromagnetic behavior with sigmoidal hysteresis curves as those typically seen in nanostructured materials with small magnetic multidomains. Despite the independence of the Co-based solid solution concentrations as identified by XRD investigation, the magnetic characteristics remain only partially stable. This suggests that due to the evolution of the amorphous phase with a small fraction of nanocrystalline phases α-Co_2B and β-Co_2Si as a solid solution, there is a single Bloch wall in magnetic domains [60].

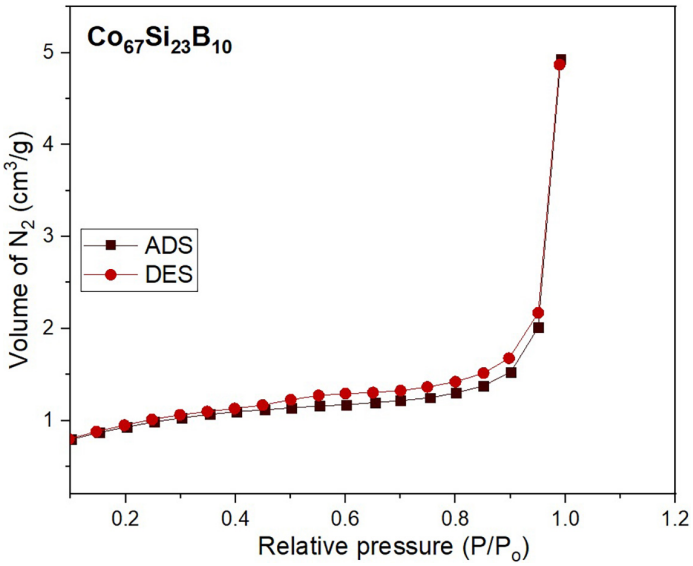

Figure 4: Adsorption/desorption isotherms of N_2 for $Co_{62}Nb_{32}B_6$ alloy.

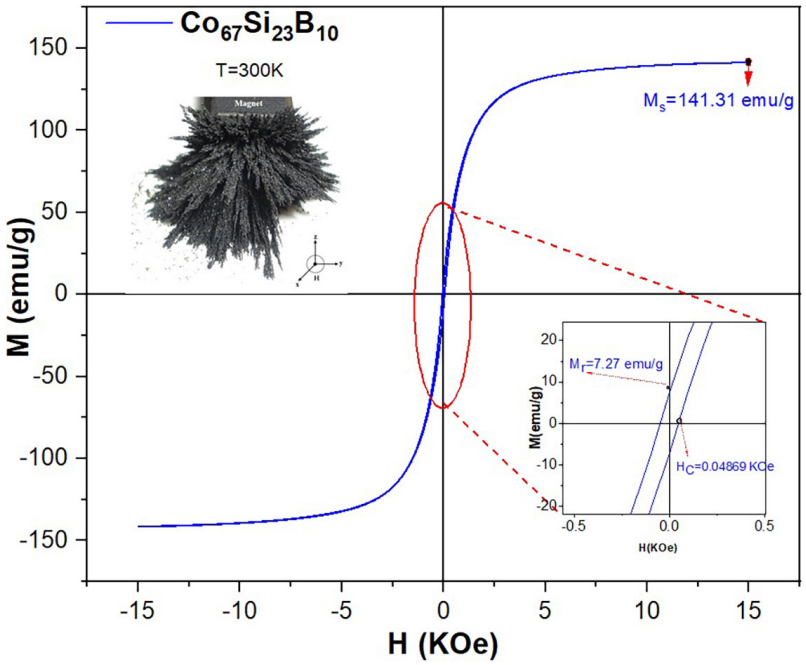

Figure 5: Hysteresis loop M-H for the powder $Co_{67}Si_{23}B_{10}$.

4. CONCLUSIONS

The α-Co_2B and β-Co_2Si nanocrystalline phases (around 1.9%) dispersed within an amorphous matrix (around 98.1%) are achieved after milling Co, Si, and B powder mixtures. This was confirmed by XRD patterns (showed the formation of a diffuse halo around 2θ = 45°, exhibiting the shape of an amorphous structure) as a function of milling time up to 15 h by MA.

The micrograph of amorphous $Co_{67}Si_{23}B_{10}$ powder showed aggregates of small powders in flake-like shapes and small spherical particles flattened with a size of 50μm, along with the-EDS analysis and mapping of the powder obtained from 15 h of milling. Co, Si, and B were present in the initial mixture, as indicated by the EDS analysis. However, the EDS mapping reveals that the powders became inhomogeneous, with distinct clusters of Co and Si indicating the development of the nanocrystalline phases α-Co_2B and β-Co_2Si coexisting with the amorphous phase towards the end result of the powder mixture's milling. The $Co_{67}Si_{23}B_{10}$ powder exhibited typical soft magnetic properties. Conversely, the $Co_{67}Si_{23}B_{10}$ powder showed two crystallization exothermic peaks at primary and secondary temperatures.

The formation of nanocrystalline phases α-Co_2B and β-Co_2Si from the amorphous phase is observed during the oxidation process at high temperatures, resulting in some mass gains. The N_2 adsorption-desorption isotherm of $Co_{67}Si_{23}B_{10}$ powder alloy represents a type IV isotherm with a hysteresis loop profile characteristic of H3 type mesoporous materials. The saturation magnetization was M_s = 114.31 emu/g, remanent magnetization was M_r = 7.27 emu/g, a coercive field H_c = 0.04869 kOe, and it showed a saturation remanence ratio in the order of M_r/M_s = 0.051447, revealing multidomains ($M_r/M_s << 0.1$) during 15 h of milling.

5. ACKNOWLEDGEMENTS

The authors wish to thank CAPES for the financial support of this researcher.

6. BIBLIOGRAPHY

[1] KANG, J., YANG, X., HU, Q., *et al.*, "Recent progress of amorphous nanomaterials", *Chemical Reviews*, v. 123, n. 13, pp. 8859–8941, 2023. doi: http://doi.org/10.1021/acs.chemrev.3c00229. PubMed PMID: 37358266.

[2] NISHIO, K., LU, A.K.A., "Unveiling a medium-range structural commonality of amorphous alloys", *Journal of Non-Crystalline Solids*, v. 624, pp. 122696, 2024. doi: http://doi.org/10.1016/j.jnoncrysol.2023.122696.

[3] NYKYRUY, Y., MUDRY, S., SHTABLAVYI, I., *et al*., "Formation of laser-induced periodic surface structures on amorphous Fe-and Co-based alloys and its impact on magnetic properties", *Materials Chemistry and Physics*, v. 287, pp. 126317, 2022. doi: http://doi.org/10.1016/j.matchemphys.2022.126317.

[4] TAN, Y., WANG, Y.W., CHENG, X.W., *et al*., "Effects of Al replacement on glass forming ability and mechanical properties of Zr-based bulk metallic glasses", *Journal of Non-Crystalline Solids*, v. 568, pp. 120962, 2021. doi: http://doi.org/10.1016/j.jnoncrysol.2021.120962.

[5] HUANG, B., ZHANG, C., ZHANG, G., *et al*., "Wear and corrosion resistant performance of thermal-sprayed Fe-based amorphous coatings: a review", *Surface and Coatings Technology*, v. 377, pp. 124896, 2019. doi: http://doi.org/10.1016/j.surfcoat.2019.124896.

[6] SUN, Y., ZHANG, X., NAN, T., *et al*., "Air surface crystallization with quenched-in Fe crystallites and associated magnetomechanical properties in Fe–Si–B amorphous ribbons", *AIP Advances*, v. 13, n. 11, pp. 115120, 2023. doi: http://doi.org/10.1063/5.0175483.

[7] GUNDEROV, D., ASTANIN, V., "Influence of HPT deformation on the structure and properties of amorphous alloys", *Metals*, v. 10, n. 3, pp. 415, 2020. doi: http://doi.org/10.3390/met10030415.

[8] MENG, J., ZHANG, Y., YU, X., *et al*., "In vivo biodegradation and biological properties of a Mg-Zn-Ca amorphous alloy for bone defect repair", *Materials Technology*, v. 39, n. 1, pp. 2307846, 2024. doi: http://doi.org/10.1080/10667857.2024.2307846.

[9] NEMATOV, M.G., BARABAN, I., YUDANOV, N.A., *et al*., "Evolution of the magnetic anisotropy and magnetostriction in Co-based amorphous alloys microwires due to current annealing and stress-sensory applications", *Journal of Alloys and Compounds*, v. 837, pp. 155584, 2020. doi: http://doi.org/10.1016/j.jallcom.2020.155584.

[10] ZHANG, X.L., WU, Y., LIU, R.R., *et al*., "A study of crystallization behavior and magnetic property of Co-based alloy", *Journal of Non-Crystalline Solids*, v. 619, pp. 122562, 2023. http://doi.org/10.1016/j.jnoncrysol.2023.122562.

[11] SKULKINA, N.A., NEKRASOV, E.S., "Nonuniformity of magnetization processes of a Co-based amorphous alloy ribbon in the As-Quenched State", *The Physics of Metals and Metallography*, v. 124, n. 8, pp. 774–780, 2023. doi: http://doi.org/10.1134/S0031918X23601117.

[12] PERMYAKOVA, I., GLEZER, A., "Mechanical behavior of Fe-and Co-based amorphous alloys after thermal action", *Metals*, v. 12, n. 2, pp. 297, 2022. doi: http://doi.org/10.3390/met12020297.

[13] KOENIG, A.G., LEARY, A., NOEBE, R., *et al*., "Crystallization characteristics in Co-based magnetic amorphous nanocomposites", *Journal of Physics and Chemistry of Solids*, v. 180, pp. 111430, 2023. doi: http://doi.org/10.1016/j.jpcs.2023.111430.

[14] JIANG, J., LI, Q., DUAN, H., *et al*., "The effects of metalloid elements (P, C, B) on the properties of Co-based amorphous alloys studied by ab initio molecular dynamics simulations", *Computational Materials Science*, v. 130, pp. 76–83, 2017. doi: http://doi.org/10.1016/j.commatsci.2016.12.042.

[15] ZHANG, W., WANG, J., ZHANG, T., *et al*., "Novel Fe–B–P–C–Cu–Co amorphous/nanocrystalline alloys with excellent comprehensive performance via Co substitution for Fe", *Intermetallics*, v. 169, pp. 108305, 2024. doi: http://doi.org/10.1016/j.intermet.2024.108305.

[16] ÖZTÜRK, S., İCIN, K., GENÇTÜRK, M., *et al*., "Surface and structural characterization of amorphous Fe, Co-based melt-spun ribbons subjected to heat treatment processes", *Journal of Non-Crystalline Solids*, v. 522, pp. 119592, 2019. doi: http://doi.org/10.1016/j.jnoncrysol.2019.119592.

[17] KUŚ, A., PILARCZYK, W., MAŁACHOWSKA, A., *et al*., "Investigation of mechanical and magnetic properties of co-based amorphous powders obtained by atomization", *Materials (Basel)*, v. 14, n. 23, pp. 7357, 2021. doi: http://doi.org/10.3390/ma14237357. PubMed PMID: 34885509.

[18] HAJIPOUR, M., RAANAEI, H., ZAREI, S., "Magnetic, morphological and thermal studies of nanostructured cobalt-based Co-Fe-Zr-Cu alloy prepared by mechanical alloying", *Journal of Magnetism and Magnetic Materials*, v. 548, pp. 168992, 2022. doi: http://doi.org/10.1016/j.jmmm.2021.168992.

[19]. LIU, R., MA, M., ZHANG, X., "New development of research on casting of bulk amorphous alloys", *Acta Metall Sin*, v. 57, n. 4, pp. 515–528, 2021. doi: http://doi.org/10.11900/0412.1961.2020.00414

[20] RYABTSEV, S.I., POLONSKYY, V.A., SUKHOVA, O.V., "Effect of scandium on the structure and corrosion properties of vapor-deposited nanostructured quasicrystalline Al–Cu–Fe films", *Powder Metallurgy and Metal Ceramics*, v. 58, n. 9, pp. 567–575, 2020. doi: http://doi.org/10.1007/s11106-020-00111-2.

[21] TAO, X., ZHANG, Z., ZHANG, B., *et al*., "Plasma sprayed CoNiCrMoNb (BSi) high-entropy amorphous alloy coating: The effect of spraying power on microstructure, mechanical and tribological properties", *Materials Chemistry and Physics*, v. 314, pp. 128887, 2024. doi: http://doi.org/10.1016/j.matchemphys.2024.128887.

[22] AVAR, B., CHATTOPADHYAY, A.K., SIMSEK, T., *et al*., "Synthesis and characterization of amorphous-nanocrystalline $Fe_{70}Cr_{10}Nb_{10}B_{10}$ powders by mechanical alloying", *Applied Physics. A, Materials Science & Processing*, v. 128, n. 6, pp. 537, 2022. doi: http://doi.org/10.1007/s00339-022-05680-0.

[23] CHEBLI, A., CESNEK, M., DJEKOUN, A., *et al*., "Synthesis, characterization and amorphization of mechanically alloyed $Fe_{75}Si_{12}Ti_6B_7$ and $Fe_{73}Si_{15}Ti_5B_7$ powders", *Journal of Materials Science*, v. 57, n. 26, pp. 12600–12615, 2022. doi: http://doi.org/10.1007/s10853-022-07404-4.

[24] YAKIN, A., SIMSEK, T., AVAR, B., *et al*., "A review of soft magnetic properties of mechanically alloyed amorphous and nanocrystalline powders", *Emergent Materials*, v. 6, n. 2, pp. 453–481, 2023. doi: http://doi.org/10.1007/s42247-023-00485-0.

[25] GHOBRIAL, S., KIRK, D.W., THORPE, S.J., "Solid state amorphization in the Ni-Nb-Y system by mechanical alloying", *Journal of Non-Crystalline Solids*, v. 502, pp. 1–8, 2018. doi: http://doi.org/10.1016/j.jnoncrysol.2018.10.015.

[26] LI, B.Y., LI, A.C., ZHAO, S., *et al*., "Amorphization by mechanical deformation", *Materials Science and Engineering R Reports*, v. 149, pp. 100673, 2022. doi: http://doi.org/10.1016/j.mser.2022.100673.

[27] NASCIMENTO, L., MORAIS, Í.C.G., SILVA, A.L., *et al*., "The powder of $Co_{64}Nb_{30}B_6$ obtained by mechanical alloying", *Quimica Nova*, v. 47, n. 8, pp. e-20240030, 2024. doi: http://doi.org/10.21577/0100-4042.20240030.

[28] MO, M., TANG, J., ZOU, L., *et al*., "Improvement and regeneration of Co–B amorphous alloy nanowires for the selective hydrogenation of cinnamaldehyde", *RSC Advances*, v. 12, n. 51, pp. 33099–33107, 2022. doi: http://doi.org/10.1039/D2RA05595C. PubMed PMID: 36425172.

[29] RHO, I.C., YOON, C.S., KIM, C.K., *et al*., "Crystallization of amorphous alloy $Co_{68}Fe_4Cr_4Si_{13}B_{11}$", *Materials Science and Engineering B*, v. 96, n. 1, pp. 48–52, 2002. doi: http://doi.org/10.1016/S0921-5107(02)00339-2.

[30] ABROSIMOVA, G., VOLKOV, N., ORLOVA, N., *et al*., "BCC nanocrystal formation in an amorphous Co-Si-B-Fe-Nb alloy on heating", *Materials Letters*, v. 219, pp. 97–99, 2018. doi: http://doi.org/10.1016/j.matlet.2018.02.069.

[31] ACKLAND, K., MASOOD, A., KULKARNI, S., *et al*., "Ultra-soft magnetic Co-Fe-B-Si-Nb amorphous alloys for high frequency power applications", *AIP Advances*, v. 8, n. 5, pp. 056129, 2018. doi: http://doi.org/10.1063/1.5007707.

[32] ZHANG, S., PENG, Z., SHI, M., *et al*., "Effects of oxygen addition on properties of an amorphous Co–Ta–B system", *Physica E, Low-Dimensional Systems and Nanostructures*, v. 154, pp. 115785, 2023. doi: http://doi.org/10.1016/j.physe.2023.115785.

[33] ZHOU, Y., WANG, T., "High stability and high corrosion resistance of a class of Co–Cr–Mo–Nb–B high-entropy metallic glasses", *Journal of Materials Research and Technology*, v. 30, pp. 256–266, 2024. doi: http://doi.org/10.1016/j.jmrt.2024.03.035.

[34] NYKYRUY, Y., MUDRY, S., KULYK, Y., *et al*., "Magnetic properties and nanocrystallization behavior of Co-based amorphous alloy", *Physics and Chemistry of Solid State*, v. 24, n. 1, pp. 106–113, 2023. doi: http://doi.org/10.15330/pcss.24.1.106-113.

[35] MSETRA, Z., KHITOUNI, N., SUÑOL, J.J., *et al*., "Characterization and thermal analysis of new amorphous $Co_{60}Fe_{18}Ta8B_{14}$ alloy produced by mechanical alloying", *Materials Letters*, v. 292, pp. 129532, 2021. doi: http://doi.org/10.1016/j.matlet.2021.129532.

[36] MOVAHEDI, B., ENAYATI, M.H., WONG, C.C., "Study on nanocrystallization and amorphization in Fe–Cr–Mo–B–P–Si–C system during mechanical alloying", *Materials Science and Engineering B*, v. 172, n. 1, pp. 50–54, 2010. doi: http://doi.org/10.1016/j.mseb.2010.04.016.

[37] PEREPEZKO, J.H., HEBERT, R.J., WILDE, G., "Synthesis of nanostructures from amorphous and crystalline phases", *Materials Science and Engineering A*, v. 375, pp. 171–177, 2004. doi: http://doi.org/10.1016/j.msea.2003.10.164.

[38] ARIK, H., TURKER, M., "Production and characterization of in situ Fe–Fe_3C composite produced by mechanical alloying", *Materials & Design*, v. 28, n. 1, pp. 140–146, 2007. doi: http://doi.org/10.1016/j.matdes.2005.05.007.

[39] GAO, Q., JIAN, Z., "Isothermal phase transformation of $Zr_{50}Cu_{43}Ag_7$ amorphous alloy", *Materials Today. Communications*, v. 36, pp. 106766, 2023. doi: http://doi.org/10.1016/j.mtcomm.2023.106766.

[40] KUMAR, A., NAYAK, S.K., BANERJEE, A., *et al*., "Multi-scale indentation creep behavior in Fe-based amorphous/nanocrystalline coating at room temperature", *Materials Letters*, v. 283, pp. 128768, 2021. doi: http://doi.org/10.1016/j.matlet.2020.128768.

[41] TAO, Z.X., LI, L.Z., WU, X.H., *et al*., "Structural, magnetic and electrical properties of CoSi ferrites synthesized by sol-gel self-propagating method", *Physica B, Condensed Matter*, v. 604, pp. 412655, 2021. http://doi.org/10.1016/j.physb.2020.412655.

[42] ZHANG, Y., ZHANG, B., LI, K., *et al*., "Electromagnetic interference shielding effectiveness of high entropy AlCoCrFeNi alloy powder laden composites", *Journal of Alloys and Compounds*, v. 734, pp. 220–228, 2018. doi: http://doi.org/10.1016/j.jallcom.2017.11.044.

[43] LI, C., PIAO, Y., MENG, B., *et al*., "Phase transition and plastic deformation mechanisms induced by self-rotating grinding of GaN single crystals", *International Journal of Machine Tools & Manufacture*, v. 172, pp. 103827, 2022. doi: http://doi.org/10.1016/j.ijmachtools.2021.103827.

[44] PĘKAŁA, M., JACHIMOWICZ, M., FADEEVA, V.I., *et al*., "Phase transformations in Co–B–Si alloys induced by high-energy ball milling", *Journal of Non-Crystalline Solids*, v. 287, n. 1–3, pp. 360–365, 2001. doi: http://doi.org/10.1016/S0022-3093(01)00596-8.

[45] NYKYRUY, Y., MUDRY, S., KULYK, Y., *et al*., "Magnetic properties and nanocrystallization process in Co–(Me)–Si–B amorphous ribbons", *Applied Nanoscience*, v. 13, n. 7, pp. 5239–5249, 2023. doi: http://doi.org/10.1007/s13204-022-02746-6.

[46] MUHGALIN, V.V., DOROFEEV, G.A., EREMINA, M.A., *et al*., "Nanocrystallization of the amorphous Co-B-Si alloys formed by melt spinning and mechanical alloying", *The Physics of Metals and Metallography*, v. 112, n. 6, pp. 596–602, 2011. doi: http://doi.org/10.1134/S0031918X11060081.

[47]. FERNANDEZ BARQUIN, L., BARANDIARAN, J.M., TELLERIA, I., *et al*., Evolution of the electrical resistivity during the crystallization of Co-Si-B glasses. *Physica Status Solidi (a)*, v. 155, n. 2, pp. 439–450, 1996.

[48] BORMIO-NUNES, C., NUNES, C.A., COELHO, A.A., *et al*., "Magnetization studies of binary and ternary Co-rich phases of the Co–Si–B system", *Journal of Alloys and Compounds*, v. 508, n. 1, pp. 5–8, 2010. doi: http://doi.org/10.1016/j.jallcom.2010.08.019.

[49] NOWOSIELSKI, R., ZAJDEL, A., BARON, A., *et al*., "Influence of crystallisation anamorphous Co_{77} $Si_{11.5}$ $B_{11.5}$ alloy on corrosion behavior", *Journal of Achievements in Materials and Manufacturing Engineering*, v. 20, n. 1–2, pp. 167–170, 2007.

[50] OLESZAK, D., MATYJA, H., "Ball milling of $Co_{70}Fe_8Si_9B_{13}$ amorphous ribbon, crystallized ribbon and a mixture of pure crystalline powders", *Journal of Materials Science*, v. 29, n. 15, pp. 4070–4074, 1994. doi: http://doi.org/10.1007/BF00355972.

[51] BREKHARYA, G., KUTSEVA, N., BASHEV, V., *et al*., "Stability of amorphous structures of nearly zero magnetostriction Co-rich microwires", *Journal of Magnetism and Magnetic Materials*, v. 249, n. 1–2, pp. 104–107, 2002. doi: http://doi.org/10.1016/S0304-8853(02)00514-0.

[52]. KUMAR, S., SHARMA, A., GAUTAM, D., *et al*., "Characterization of mesoporous materials. advanced functional porous materials: from macro to nano scale lengths", In: Uthaman, A., Thomas, S., Li, T., Hanna Maria, H. (eds), *Advanced Functional Porous Materials*, Springer Nature title, pp. 175–204, 2022.

[53] NASCIMENTO, L., LEAL, E., DA SILVA, A.L., *et al*., "Evaluation of the microstructure and magnetic properties of amorphous $Co_{62}Nb_{32}B_6$ alloy produced by mechanical alloying", *Brazilian Journal of Physics*, v. 54, n. 3, pp. 87, 2024. doi: http://doi.org/10.1007/s13538-024-01467-1.

[54] GAO, C., TANG, S., ZHAO, S., *et al*., "Amorphous/crystalline $Zn_{60}Zr_{40}$ alloys lattice structures with improved mechanical properties fabricated by mechanical alloying and selective laser melting", *Virtual and Physical Prototyping*, v. 18, n. 1, pp. e2220549, 2023. doi: http://doi.org/10.1080/17452759.2023.2220549.

[55] OH, H.S., XU, M., WEI, S., *et al*., "Composition-dependent transformation-induced plasticity in Co-based complex concentrated alloys", *Acta Materialia*, v. 262, pp. 119349, 2024. doi: http://doi.org/10.1016/j.actamat.2023.119349.

[56] LAUNEY, M.E., BUSCH, R., KRUZIC, J.J., "Effects of free volume changes and residual stresses on the fatigue and fracture behavior of a Zr–Ti–Ni–Cu–Be bulk metallic glass", *Acta Materialia*, v. 56, n. 3, pp. 500–510, 2008. doi: http://doi.org/10.1016/j.actamat.2007.10.007.

[57] LIU, Y., YI, Y., SHAO, W., *et al*., "Microstructure and magnetic properties of soft magnetic powder cores of amorphous and nanocrystalline alloys", *Journal of Magnetism and Magnetic Materials*, v. 330, pp. 119–133, 2013. doi: http://doi.org/10.1016/j.jmmm.2012.10.043.

[58] KHITOUNI, N., HAMMAMI, B., LLORCA-ISERN, N., *et al*., "Microstructure and magnetic properties of nanocrystalline $Fe_{60-x}Co_{25}Ni_{15}Si_x$ alloy elaborated by high-energy mechanical milling", *Materials (Basel)*, v. 15, n. 18, pp. 6483, 2022. doi: http://doi.org/10.3390/ma15186483. PubMed PMID: 36143795.

[59] HAFS, A., HAFS, T., BERDJANE, D., *et al*., "Magnetic properties, phase evolution, and microstructure of $fe_{90}nb_{10}$ powder mixtures", *Journal of Superconductivity and Novel Magnetism*, pp. 1–16, 2024. doi: http://doi.org/10.1007/s10948-024-06740-7.

[60] DALY, R., KHITOUNI, N., ESCODA, M.L., *et al*., "Microstructure, magnetic and Mössbauer studies of mechanically alloyed FeCoNi nanocrystalline powders", *Arabian Journal for Science and Engineering*, v. 46, n. 6, pp. 5633–5643, 2021. doi: http://doi.org/10.1007/s13369-020-05166-2.